energies

MDPI

Article

Improving Carrier Transport Behavior in a Bilayer ETL for Enhanced Efficiency of Perovskite Solar Cells: An Investigation

Rui-Yun Hsu [1,*], Yeong-Lin Lai [2,*], Yung-Hua Chou [2] and Wei-Jhe Syu [2]

[1] Department of Electrical Engineering, National University of Kaohsiung, Kaohsiung 811, Taiwan
[2] Department of Mechatronics Engineering, National Changhua University of Education, Changhua 500, Taiwan
* Correspondence: ryhsu@nuk.edu.tw (R.-Y.H.); yllai@cc.ncue.edu.tw (Y.-L.L.)

Abstract: Perovskite solar cells (PSCs) are currently among the most promising solar cell technologies. A key component influencing their efficiency and stability is the electron transport layer (ETL). This study examined the carrier transport properties of various ETL materials, including TiO_2, SnO_2, and TiO_2/SnO_2 bilayer ETLs, to understand their effects on PSC performance. The study proposed a hypothesis that the bilayer design, integrating TiO_2 and SnO_2, enhances performance, and it used experimental results to substantiate this. Through analysis and discussion of the ETLs, the interface between perovskite (PVSK) and ETLs, and other PSC components, we gained insights into the carrier transport dynamics in PSCs with different ETL configurations. Our findings indicate that the TiO_2/SnO_2 bilayer ETL structure can significantly improve PSC performance by reducing current leakage, improving carrier transport, and minimizing carrier recombination. This enhancement is quantified by the increase in efficiency from 13.58% with a single-layer TiO_2 ETL to 20.49% with the bilayer ETL.

Keywords: perovskite; bilayer ETL; solar cell

Citation: Hsu, R.-Y.; Lai, Y.-L.; Chou, Y.-H.; Syu, W.-J. Improving Carrier Transport Behavior in a Bilayer ETL for Enhanced Efficiency of Perovskite Solar Cells: An Investigation. *Energies* **2024**, *17*, 871. https://doi.org/10.3390/en17040871

Academic Editor: Philippe Leclère

Received: 3 October 2023
Revised: 29 January 2024
Accepted: 30 January 2024
Published: 13 February 2024

1. Introduction

Perovskite solar cells (PSCs) have garnered considerable attention in recent years due to their excellent material properties, which have resulted in significant increases in their conversion efficiencies [1–3]. Over the past decade, the power conversion efficiencies (PCEs) of PSCs have increased from 3.8% [4] to a remarkable 25.5% [5–7], which is approaching the efficiency record of silicon solar cells at 26.7% [8]. This advance puts PSCs at the forefront of next-generation solar cell technologies, offering not only high efficiency but also low cost [9,10]. As a result of these advantages, PSCs have the potential to be widely used in solar energy applications and to help to reduce reliance on fossil fuels [11,12].

PSCs are typically composed of a transparent electrode, an electron transport layer (ETL), an absorber layer, a hole transport layer (HTL), and a metal electrode. In pursuit of high-performance PSCs, ETL has become one of the highly researched topics [13]. TiO_2 is currently the most commonly used ETL material; however, it causes degradation of the perovskite (PVSK) under UV light, which leads researchers to explore alternative materials with better optoelectronic properties to replace TiO_2. Due to its high electron mobility, high conductivity, wide optical bandgap, and excellent chemical stability, SnO_2 has emerged as one of the most studied ETL materials after TiO_2 [14,15]. However, the lower conduction band of the SnO_2 ETL reduces the built-in potential of the Schottky barrier between PVSK and SnO_2, affecting the collection of carriers at the PVSK/SnO_2 interface and reducing the open-circuit voltage (V_{oc}) of PSCs [16].

In recent years, researchers have started using bilayer ETL structures to improve the efficiency of PSCs, and related studies can be summarized into the following findings: (1) The development of TiO_2/SnO_2 bilayer ETLs has encompassed various structures [17],

fabrication techniques [18,19], and doping strategies [20,21]. (2) Combining TiO_2/SnO_2 bilayer ETLs with various PVSK materials enhances the performance and stability of PSCs [22,23]. (3) The mechanism of improving the light stability of PSCs using TiO_2/SnO_2 bilayer ETL has been investigated [24]. Although the use of TiO_2/SnO_2 bilayer structures has achieved some success in improving the efficiency of PSCs, an understanding of the carrier transport mechanisms and defect mitigation of TiO_2/SnO_2 bilayer ETL at the ETL/PVSK interface remains incomplete.

To gain a deeper understanding of various ETLs such as TiO_2, SnO_2, and TiO_2/SnO_2 bilayer ETLs, and their impact on perovskite solar cells (PSCs), this study embarks on a detailed exploration. The focus is on analyzing the carrier transport and defect characteristics at the ETL/perovskite interface, and how these influence the efficiency of PSCs. This is achieved through a comprehensive study of the ETL itself, the ETL/perovskite interface, and their collective effect on PSC performance. The methodology includes examining the ETLs using scanning electron microscopy (SEM) and conductive atomic force microscopy (C-AFM). These techniques provide insights into the structure and function of the TiO_2/SnO_2 bilayer ETL, particularly in relation to current leakage suppression. Additionally, this study utilizes photoluminescence (PL) quenching and time-resolved photoluminescence (TR-PL) analyses. These methods are instrumental in understanding carrier transport behavior at the perovskite/ETL interface, especially in terms of how the TiO_2/SnO_2 bilayer ETL can enhance carrier transport, minimize carrier recombination due to interface defects, and thus potentially improve the PSCs' performance metrics such as the short-circuit current density (J_{sc}), fill factor (FF), and overall conversion efficiency.

2. Materials and Methods

Materials: FTO glass substrates were purchased from Ruilong Optoelectronics Technology Co., Ltd. (Miaoli, Taiwan). Zinc powder of 100 mesh (purity 97%) was obtained from Thermo Scientific (Waltham, MA, USA). Tin (II) chloride dihydrate ($SnCl_2{\cdot}2H_2O$, purity 98%) was purchased from Sigma-Aldrich (St. Louis, MO, USA), while Formamidinium iodide (FAI, purity 98%) and Methylammonium bromide (MABr, purity 99.99%) were sourced from Greatcell Solar Materials Pty Ltd. (Queanbeyan, Australia). Lead (II) bromide ($PbBr_2$, purity 99.99%) and Cesium iodide (CsI, purity 99.998%) were acquired from Alfa Aesar (Haverhill, MA, USA). Spiro-MeOTAD (purity 99%), Lithium bis (trifluoromethanesulfonyl) imide (LiTFSI, purity 99.95%), and 4-tert-butylpyridine (tBP, purity 98%) were all purchased from Sigma-Aldrich. Lead (II) Iodide (PbI_2, purity 99.99%) was obtained from TCI. Other solvents were purchased from Sigma-Aldrich or J.T. Baker (Phillipsburg, NJ, USA) and were used without further purification.

Device fabrication: The FTO glass (NSG-10) was etched with a zinc powder and HCl solution (2M) to create the desired electrode pattern. The substrates were then washed with Triton X100 (1 Vol% in deionized water), deionized water, acetone, and ethanol. Three different ETLs were then deposited on the FTO glass separately using the following methods: (1) TiO_2 ETL: The FTO glass substrate was soaked in a 70 °C 40 mM $TiCl_4$ aqueous solution for 30 min in a water bath, rinsed with deionized water, and repeatedly deposited three times. Finally, the substrate was annealed at 475 °C for 30 min to form an approximately 15–20 nm-thick TiO_2 compact layer. (2) SnO_2 ETL: $SnCl_2{\cdot}2H_2O$ powder was dissolved in an ethanol solution (0.05 M) and spin-coated at 4000 rpm for 30 s. The SnO_2 ETL was subsequently formed by annealing at 180 °C for 30 min, resulting in an approximately 25–30 nm-thick SnO_2 layer. (3) TiO_2/SnO_2 bilayer: A layer of SnO_2 was deposited on top of the deposited TiO_2 ETL to form a TiO_2/SnO_2 bilayer ETL structure. PVSK was then deposited on the ETL as an absorber layer.

For the PVSK configuration, a solution was prepared by mixing formamidine iodide (FAI, 1.105 M), PbI_2 (1.16 M), methyl ammonium bromide (MABr, 0.195 M), and $PbBr_2$ (0.195 M) together and dissolving them in a mixed solvent of DMF:DMSO = 4:1 (volume ratio). A 5 Vol% CsI solution (1.5 M in DMSO) was then added to make a ternary cation PVSK solution. The PVSK solution was spin-coated on the above three kinds of ETL

substrates separately at 1000 rpm for 10 s and 4000 rpm for 30 s. Chlorobenzene (200 µL) was dropped on the substrate 15 s before the end of the rotation, and then the substrate was annealed at 100 °C for 60 min to form a PVSK absorber layer with a thickness of approximately 550 nm. The cross-sectional SEM image of the PVSK with the bilayer ETL on the FTO glass is shown in Figure S1 of Supplementary Materials.

Spiro-OMeTAD was then deposited as an HTL. The spiro-OMeTAD powder was dissolved in 1 mL of chlorobenzene (70 mM), and 18 µL of bis(trifluoromethylsulfonyl)imide lithium salt (Li-TFSI), dissolved in acetonitrile (520 mg/1 mL), and 33 µL of 4-tert-butylpyridine (tBP) solution were added. The spiro-OMeTAD solution was then spin-coated on the PVSK light-absorbing layer at 4000 rpm for 20 s, resulting in an approximately 400 nm-thick spiro-OMeTAD HTL. Finally, 80 nm-thick gold was vapor-deposited as the back electrode, completing the PSC device structure consisting of FTO/TiO_2/SnO_2/PVSK/Spiro-OMeTAD/Au.

Characterizations and Measurements: In this study, we utilized high-resolution scanning electron microscopy (HRSEM) JEOL JSM-7800F (Tokyo, Japan) to analyze the morphology of ETL films. Atomic force microscopy (AFM) Veeco D3100 (Plainview, NY, USA) and conductive atomic force microscopy (C-AFM) BRUKER Dimension Icon (Billerica, MA, USA) were used to examine the topography and carrier transmission characteristics of the ETL films. Photoluminescence (PL) and time-resolved photoluminescence (TR-PL) analyses were conducted at the perovskite/ETL interface using a 473 nm pulse laser from Omicron (Vacaville, CA, USA) and an Andor Kymera 328i spectrometer (Oxford Instruments plc, Oxfordshire, UK). The external quantum efficiency (EQE) was measured using Enlitech equipment to assess the conversion efficiency of photons into external electrons in solar cells. Additionally, space charge limited current (SCLC) and dark current measurements were performed to investigate the defect properties of perovskite solar cells (PSCs). Current–voltage measurements were conducted under 100 mW/cm^2 AM 1.5 G illumination using a Yamashita Denso YSS-100A (Tokyo, Japan) solar simulator and a Keithley 2400 power supply (Solon, OH, USA). All measurements were carried out at a constant temperature of 25 °C in an ambient environment.

3. Results and Discussion

3.1. The Properties of the Different ETLs Subsection

3.1.1. SEM Images of ETLs

The ETLs are important components in the fabrication of PSCs, as they help to transport electrons generated by the PVSK absorber layer to the electrode. In this study, the TiO_2, SnO_2, and TiO_2/SnO_2 bilayer ETLs were deposited on FTO substrates. SEM images visually compare the surface morphology of TiO_2, SnO_2, and TiO_2/SnO_2 bilayer ETLs, as shown in Figure 1. The small particles present on the surface of TiO_2 may be attributed to the aggregation of TiO_2 nanoparticles during the chemical bath deposition process. Conversely, the smoother surface of SnO_2 suggests that the spin-coating process resulted in a more uniform and homogeneous film during the formation of SnO_2. The TiO_2/SnO_2 bilayer ETL structure combines both TiO_2 and SnO_2, and the SEM image shows a surface morphology that falls in between that of TiO_2 and SnO_2 ETL. A smoother ETL surface facilitates the transport of charge carriers at the interface of PVSK and ETL.

3.1.2. AFM of ETLs

As shown in Figure 2, atomic force microscopy (AFM) was used to analyze the surface roughness of the three different ETL films deposited on FTO glass. The AFM images (with a scan area of 5 × 5 μm^2) reveal that the root-mean-square roughness (RMS) values for the TiO_2, SnO_2, and TiO_2/SnO_2 ETLs are 24.4 nm, 21.7 nm, and 22.7 nm, respectively. The results from the AFM show that the TiO_2/SnO_2 bilayer can reduce the surface roughness of TiO_2 and decrease the pinholes in the TiO_2 and SnO_2 ETLs, providing better film coverage on the electrode. This helps to reduce the leakage current generated at the ETL/electrode interface in the PSC devices.

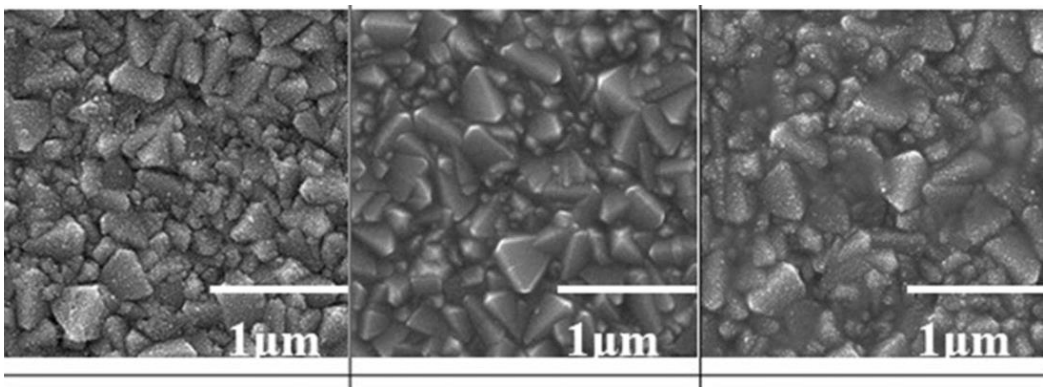

(**a**) (**b**) (**c**)

Figure 1. SEM images of (**a**) TiO_2, (**b**) SnO_2, and (**c**) TiO_2/SnO_2 bilayer ETLs deposited on FTO substrates.

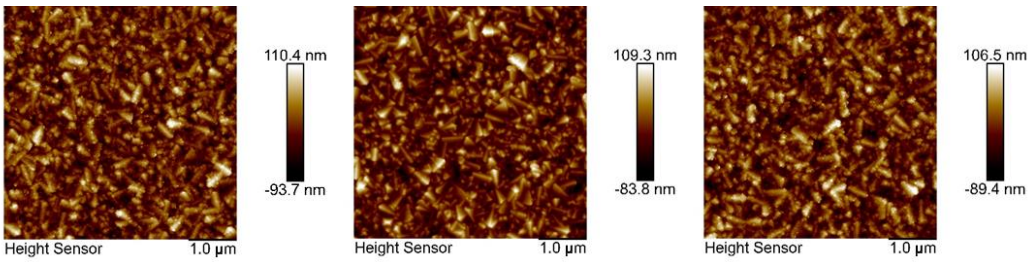

(**a**) (**b**) (**c**)

Figure 2. AFM images of (**a**) TiO_2, (**b**) SnO_2, and (**c**) TiO_2/SnO_2 bilayer ETLs deposited on FTO substrates.

3.1.3. C-AFM of ETLs

The study aimed to investigate the current leakage of different ETL materials on FTO substrates and to determine their impacts on the efficiency of PSCs. C-AFM was used to analyze the current leakage. Figure 3 shows the C-AFM images of TiO_2, SnO_2, and TiO_2/SnO_2 bilayer ETLs on an FTO substrate. The results show that SnO_2 ETL had the highest leakage current, followed by TiO_2 ETL, and the TiO_2/SnO_2 bilayer ETL had the lowest leakage current in Figure 3. The significantly lower leakage current of the bilayer structure (<4.5 pA) indicates that it can effectively reduce the current leakage of the ETL, resulting in higher FF values and efficiency of the PSCs. The results suggest that the use of a TiO_2/SnO_2 bilayer structure can improve the performance of PSCs by reducing current leakage.

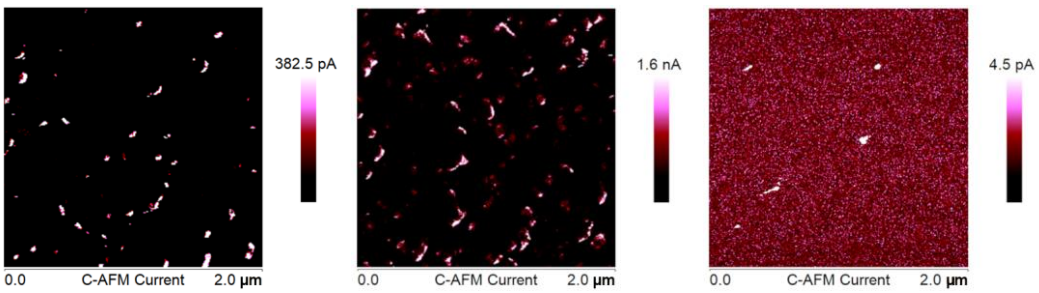

(**a**) (**b**) (**c**)

Figure 3. C-AFM images of (**a**) TiO_2, (**b**) SnO_2, and (**c**) TiO_2/SnO_2 bilayer ETLs on FTO substrates.

3.2. Carrier Transfer at the Interface of PVSK and ETLs

3.2.1. PL Quenching at PVSK/ETL Interface

PL quenching is a phenomenon that occurs when the radiative recombination of photoexcited carriers in a material is suppressed due to non-radiative recombination processes. In this study, PL quenching with an excitation wavelength of 473 nm was used to investigate the carrier transport behavior between the interfaces of PVSK and ETLs.

PVSK films were grown on different substrates, including glass, TiO_2, SnO_2, and a TiO_2/SnO_2 bilayer. The PL intensity of the films was measured. The results showed that the PVSK film grown on the glass substrate exhibited the strongest PL intensity as shown in Figure 4, indicating that carriers were effectively recombining and radiating in the PVSK film. However, when the PVSK was grown on ETLs, the PL intensity successively decreased, suggesting that carriers were more easily transported from the PVSK to the ETLs.

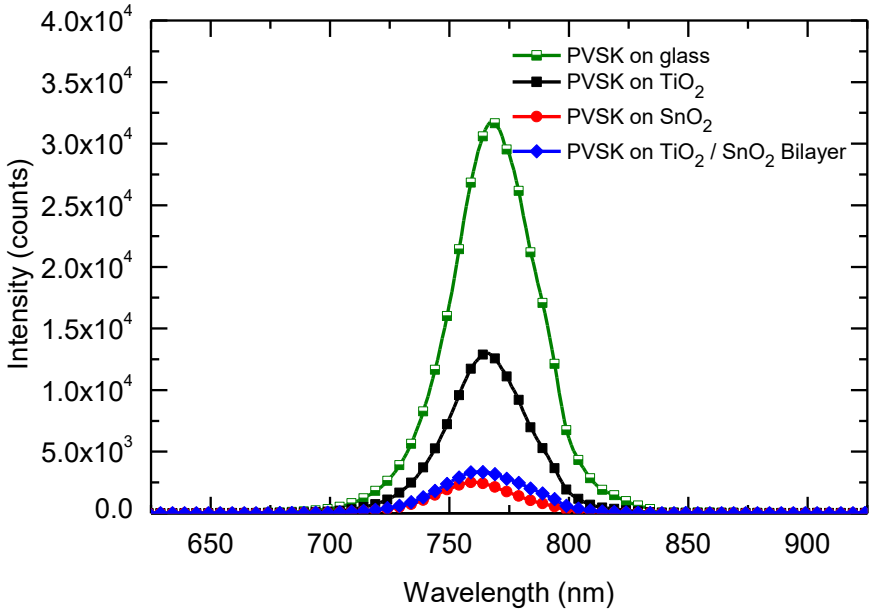

Figure 4. PL spectra of PVSK/glass, PVSK/TiO_2, PVSK/SnO_2, and PVSK/bilayer ETL interfaces.

Furthermore, the PL quenching was found to be the strongest for the PVSK film grown on the TiO_2/SnO_2 bilayer ETL, suggesting that the carrier transport between PVSK and the bilayer ETL was the most efficient. This result is consistent with the lower current leakage observed in the C-AFM analysis, indicating that the bilayer ETL can effectively reduce the leakage current of the ETL and enhance carrier transport between the PVSK and the ETL.

3.2.2. TR-PL at PVSK/ETL Interface

TR-PL spectroscopy was employed to examine the charge carrier recombination behavior and dynamics of PVSK films grown on different ETLs. An excitation wavelength of 473 nm was used, and the photoluminescence (PL) decay time and amplitude were modeled using a biexponential expression:

$$f(x) = \sum A_i e^{-\frac{t}{\tau_i}} + K \quad (1)$$

where A_i is the decay amplitude, τ_i is the decay time, and K is a constant used for the baseline offset. The average PL decay times (τ_{ave}) were then estimated using the τ_i and A_i values obtained from the fitted curve data as follows [25]:

$$\tau_{ave} = \frac{\sum A_i \tau_i^2}{\sum A_i \tau_i} \quad (2)$$

In this model, the two exponential components are interpreted to represent distinct physical processes. The first exponential component ($\tau = 1$) corresponds to the non-radiative capture of free carriers, while the second ($\tau = 2$) relates to the radiative recombination of perovskite carriers. τ_{ave} is then calculated using both τ_1 and τ_2, following Formula (2).

Figure 5 illustrates TR-PL fitting curves and the corresponding calculated lifetimes for different samples, which include PVSK/glass, PVSK/TiO_2, PVSK/SnO_2, and PVSK/bilayer. The respective lifetimes for these samples are as follows: 584.7 ns for PVSK/glass, 179.4 ns for PVSK/TiO_2, 142.6 ns for PVSK/SnO_2, and 101.9 ns for PVSK/bilayer. The TR-PL results demonstrate that the PVSK grown on glass exhibits the longest carrier lifetime. Interestingly, as different ETLs are added, the carrier lifetime in PVSK significantly decreases. This reduction can be attributed to the accelerated transfer of carriers from PVSK to ETL, leading to a decrease in carrier lifetime. The TR-PL data also indicate that the PVSK film on the TiO_2/SnO_2 bilayer ETL has the shortest carrier lifetime, suggesting that carrier transport at the PVSK/bilayer ETL interface is highly efficient. The findings reveal that the TiO_2/SnO_2 bilayer ETL can effectively promote carrier transport and minimize carrier recombination, both of which are crucial for enhancing the performance of PSCs.

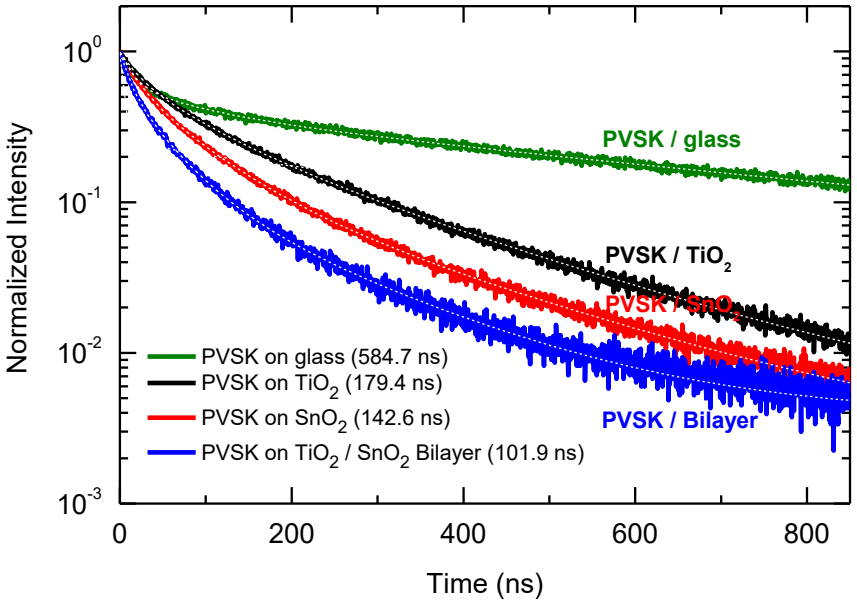

Figure 5. TR-PL spectra of PVSK/glass, PVSK/TiO_2, PVSK/SnO_2, and PVSK/bilayer interfaces.

3.3. The Impact of PSC Properties on Device Performance

3.3.1. The Dark Current of PSCs

Figure 6 shows the dark current density-applied voltage curves of PSCs grown using different ETLs under dark conditions. The results indicate that PSCs fabricated with a TiO_2/SnO_2 bilayer structure exhibit a significant reduction in dark current under negative bias, suggesting that the bilayer structure effectively suppresses the leakage current of PSCs. In fact, the leakage current densities of PSC with the bilayer ETL are one-third lower than those of the traditional SnO_2 and TiO_2 single-layer ETL, which is consistent with the C-AFM results measured for the ETLs in the previous paragraph.

In addition, the V_{oc} of a solar cell can be calculated using the equation $V_{oc} = nkT/q\ ln\ (J_{sc}/J_o)$, where n is the ideality factor, k is the Boltzmann constant, T is the temperature, q is the elementary charge, and J_{sc} and J_o are the photo-generated current density and dark saturation current density, respectively [26]. Using this equation, it was found that the bilayer ETLs structure had a lower Jo and higher J_{sc}, resulting in an increase in the value of V_{oc} of the device. This result is consistent with the *J-V* efficiency measurement results and indicates that incorporating a bilayer ETL structure in PSCs can significantly improve the V_{oc} of the device.

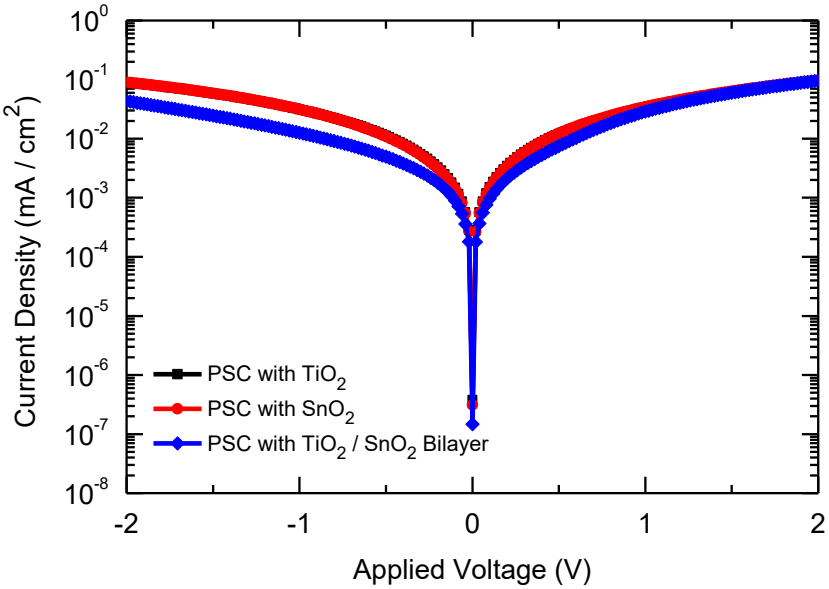

Figure 6. Dark current density-applied voltage curves of PSCs with TiO_2, SnO_2, and TiO_2/SnO_2 bilayer ETLs.

3.3.2. The SCLC Behavior in PSCs

To investigate the defect density at the interface between different ETLs and PVSK absorbers, we utilized the SCLC method for measurement. SCLC is a phenomenon of charge transport in thin films, and by analyzing the current–voltage curve, relevant parameters such as charge transport and defect density of solar cells can be obtained. In the current–voltage curve of PSCs, two regions can be distinguished: the "Ohmic region" and the "Trap-filled region"; the intersection point of these two regions is called V_{TFL} (trap-filled limit voltage) [27,28].

Figure 7 shows the V_{TFL} values for three different ETLs (TiO_2, SnO_2, and TiO_2/SnO_2) are 0.60 V, 0.54 V, and 0.39 V, respectively. The results showed that TiO_2/SnO_2ETL had the lowest V_{TFL}, indicating the smallest defect density. Finally, the defect density (N_{defect}) of the PSCs made with three different ETLs was calculated using the formula $N_{defect} = 2\,\varepsilon\varepsilon_0 V_{TFL}/eL^2$ where ε is the relative dielectric constant, ε_0 is the vacuum dielectric constant, e is the basic charge, and L is the thickness of the film [27]. The calculated results indicate that the defect densities in PSCs with TiO_2, SnO_2, and TiO_2/SnO_2 bilayer ETLs are 5.28×10^{15}, 4.75×10^{15}, and 3.43×10^{15} cm^{-3}, respectively. The results show that the PSC with TiO_2/SnO_2 ETL had the lowest defect density, confirming that the bilayer structure can effectively reduce the defect density at the interface between the ETL and PVSK and reduce radiative recombination at the interface. Therefore, reducing the defect density can improve the V_{oc}, FF, and J_{sc} of PSCs, thereby increasing the conversion efficiency of the devices.

3.3.3. The Analysis of External Quantum Efficiency (EQE) of PSCs

The external quantum efficiency (EQE) is defined as the number of free electrons (which are produced by the incident photons) collected from the device to the external circuit of the device per photon incident on it [29]. Figure 8 shows the EQE of PSCs fabricated using different ETLs. From the EQE measurement results, it can be observed that the TiO_2/SnO_2 bilayer ETL exhibits the highest EQE and photocurrent collection efficiency. As previously analyzed, the bilayer ETL structure facilitates current collection and can reduce the defects at the interface between the PVSK and the ETL, thereby increasing the J_{sc} and the efficiency of the PSCs. The integrated J_{sc} values obtained from the EQE of the devices fabricated using TiO_2, SnO_2, and TiO_2/SnO_2 ETLs were 19.33, 21.04, and 22.93 mA/cm^2, respectively, which are consistent with the J_{sc} trends simulated under illumination.

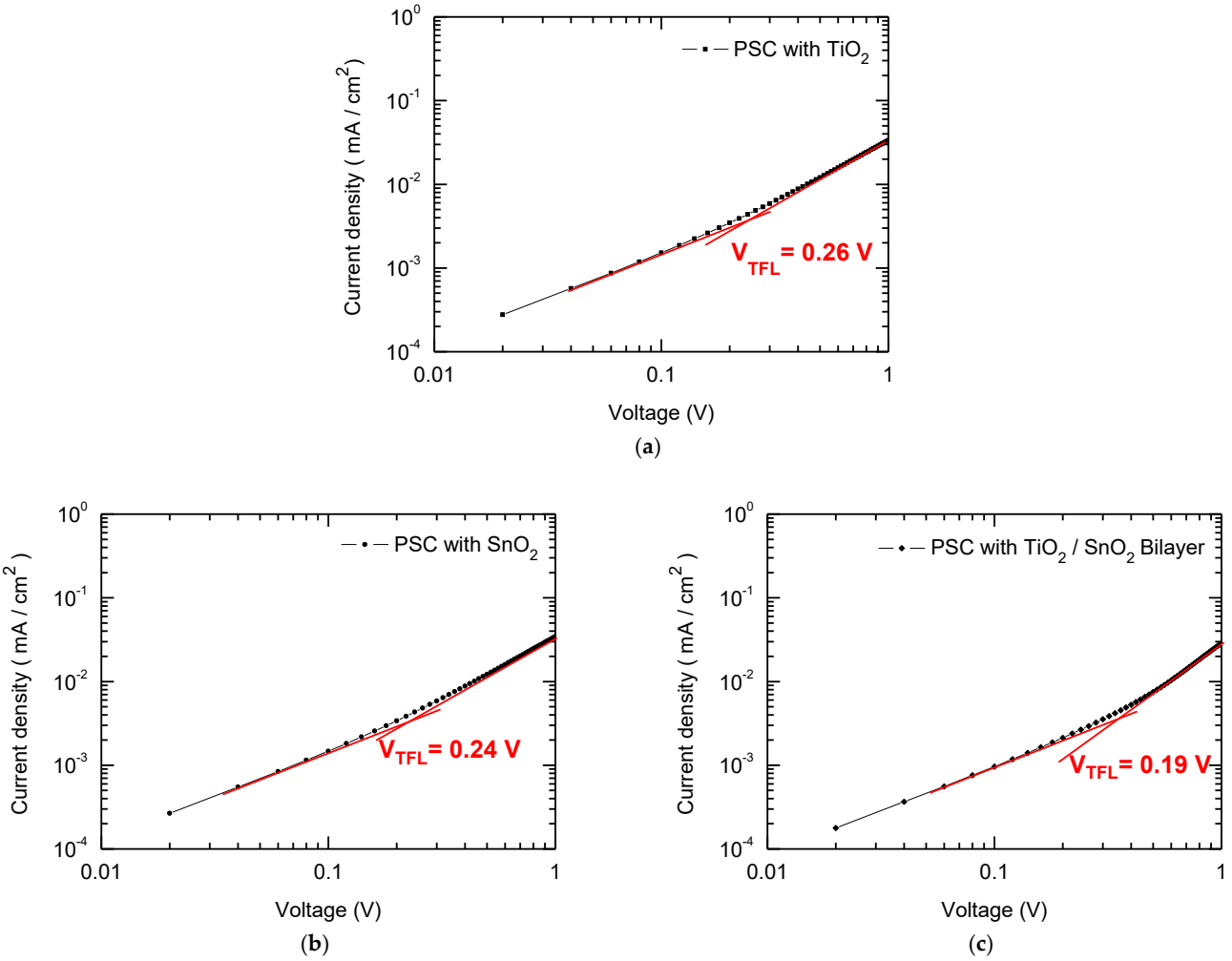

Figure 7. V_{TFL} values of the PSC devices with (**a**) TiO_2, (**b**) SnO_2, and (**c**) TiO_2/SnO_2 bilayer ETLs.

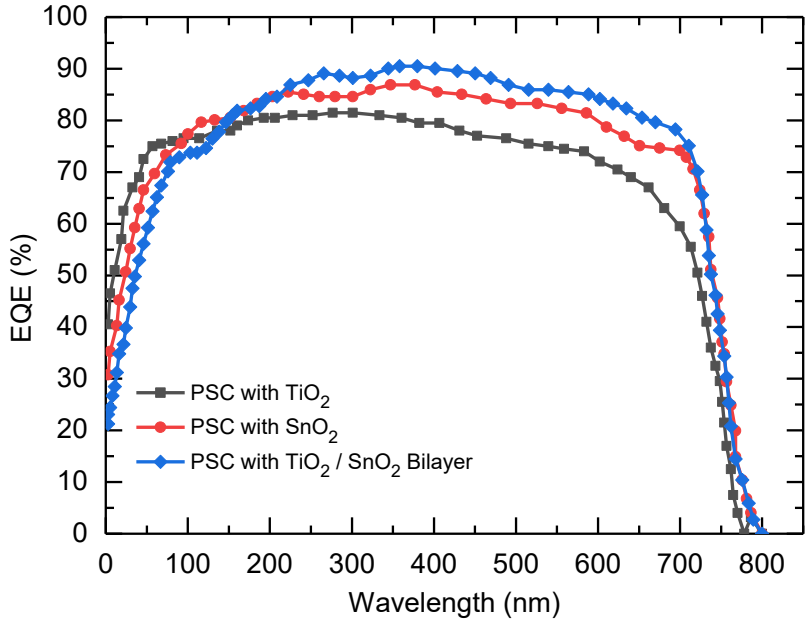

Figure 8. EQE curves of the PSC devices with TiO_2, SnO_2, and TiO_2/SnO_2 bilayer ETLs.

3.3.4. The J-V Curves Analysis of PSCs

Figure 9 presents the *J-V* curves and indicates that PSCs with a TiO_2/SnO_2 bilayer result in a higher J_{sc}, V_{oc}, and FF compared to traditional SnO_2 or TiO_2 single-layer ETLs, leading to superior PCEs for the solar cells.

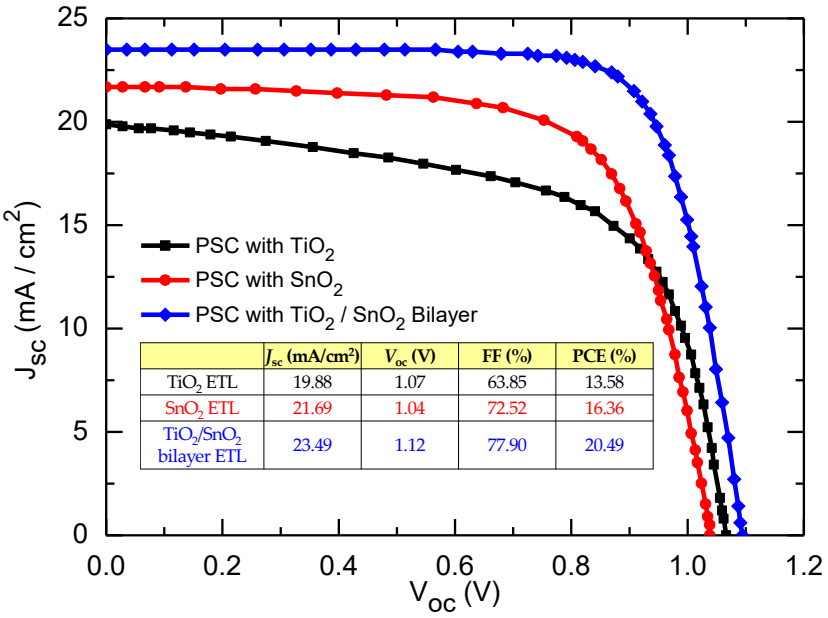

	J_{sc} (mA/cm^2)	V_{oc} (V)	FF (%)	PCE (%)
TiO_2 ETL	19.88	1.07	63.85	13.58
SnO_2 ETL	21.69	1.04	72.52	16.36
TiO_2/SnO_2 bilayer ETL	23.49	1.12	77.90	20.49

Figure 9. *J-V* curves of PSCs fabricated with TiO_2, SnO_2, and TiO_2/SnO_2 bilayer ETLs.

Based on previous PL and TR-PL analysis, it is evident that the TiO_2/SnO_2 bilayer ETL structure can effectively promote carrier transport at the interface between PVSK and the bilayer ETL. This substantially enhances the J_{sc} of PSCs, thereby resulting in a higher EQE. Additionally, C-AFM and dark current measurements corroborate the significant role of the bilayer ETL structure in reducing the leakage current in PSCs. This contributes to the improvement of both V_{oc} and FF in PSCs.

Furthermore, SCLC results illustrate that PSCs with TiO_2/SnO_2 ETL possess the lowest defect density. This finding underscores the benefits of the bilayer structure, which can effectively reduce the defect density at the interface between the ETL and PVSK and mitigate radiative recombination at the interface. The decrease in defect density directly impacts the J_{sc}, V_{oc}, and FF of PSCs, ultimately boosting the overall efficiency of PSCs.

Based on the *J-V* curve measurement results, the V_{oc} of PSCs increased from 1.07 V (TiO_2 ETL) and 1.04 V (SnO_2 ETL) to 1.12 V (bilayer ETL). The J_{sc} escalated from 19.88 mA/cm^2 (TiO_2 ETL) and 21.69 mA/cm^2 (SnO_2 ETL) to 23.49 mA/cm^2 (bilayer ETL). The FF rose from 63.85% (TiO_2 ETL) and 72.52% (SnO_2 ETL) to 77.90% (bilayer ETL). The PCE of the solar cell, with an active area of 0.45 cm^2, improved from 13.58% (TiO_2 ETL) and 16.36% (SnO_2 ETL) to 20.49% (bilayer ETL).

In conclusion, the bilayer ETL structure plays a pivotal role in enhancing the J_{sc}, V_{oc}, and FF of PSC components, thereby bolstering the conversion efficiency of the devices.

3.3.5. The Statistical Distribution of PSCs

To study reproducibility, we evaluated 16 independent PSCs fabricated using three different ETLs. Figure 10a–d show the histograms of the statistical distribution for PSCs based on different ETLs. Notably, compared to traditional single-layer ETLs, the PSCs based on the TiO_2/SnO_2 bilayer ETL exhibit higher average J_{sc}, V_{oc}, FF, and efficiency values of 23.08 ± 0.5 mA cm^2, 1.12 ± 0.01 V, 0.77 ± 0.02, and 19.8 ± 0.6%, respectively. These results demonstrate that the TiO_2/SnO_2 bilayer ETL has significant advantages in improving the J_{sc}, V_{oc}, FF, and power conversion efficiency of PSCs.

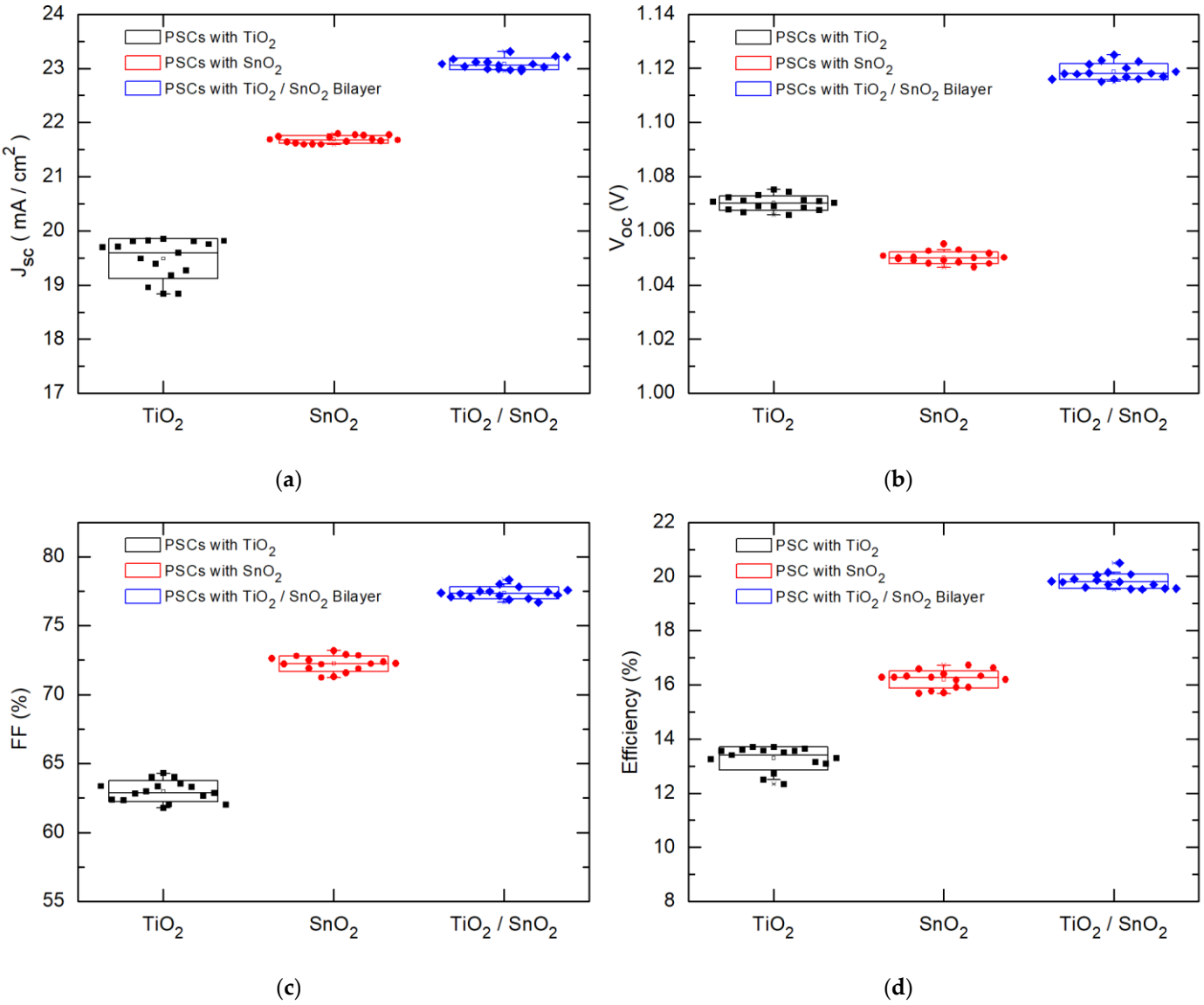

Figure 10. The statistical distribution of (**a**) J_{sc}, (**b**) V_{oc}, (**c**) FF, and (**d**) efficiency of PSCs fabricated with TiO_2, SnO_2, and TiO_2/SnO_2 bilayer ETLs.

3.3.6. The Defect Compensation Mechanism of the TiO_2/SnO_2 Bilayer ETL

According to the analysis above, when TiO_2 is used as the ETL, many defects are generated within the film, which leads to carrier recombination and leakage current in the PSC, thereby affecting the efficiency of the device. When SnO_2 is used as the ETL, its energy gap matching with the PVSK absorption is not ideal and it cannot perfectly cover the FTO electrode, which affects the V_{oc} of the device and leads to localized short-circuit phenomena, further affecting the current collection and efficiency of the PSC. However, when using a TiO_2/SnO_2 bilayer structure, SnO_2 effectively reduces the surface defects of TiO_2, as shown in Figure 11, and can better adjust the energy gap matching with the PVSK absorption, which helps to improve the carrier collection efficiency and further increase the J_{sc} and FF of the PSC, thereby significantly improving the efficiency of the device. In addition, the TiO_2/SnO_2 bilayer structure also improves the photocatalytic phenomenon between TiO_2 and the PVSK interface under UV light irradiation, thus improving the stability and durability of the PSC [23].

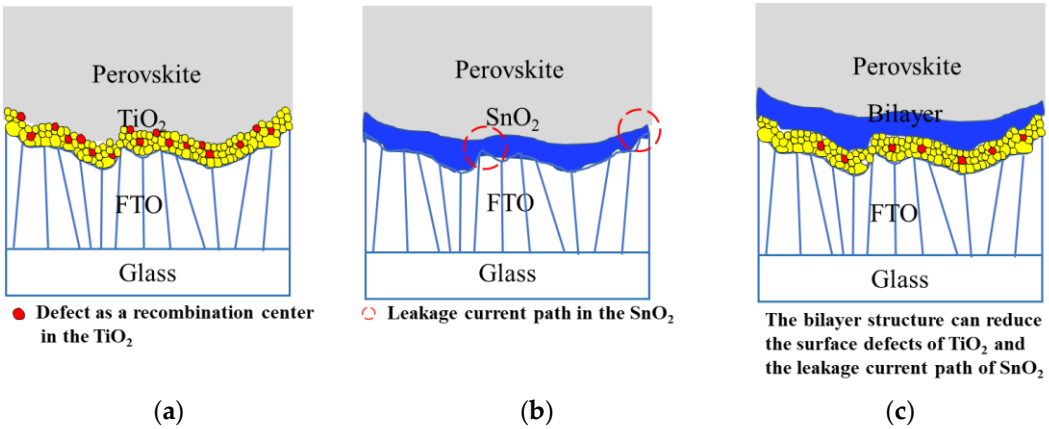

Figure 11. Schematic diagrams of (**a**) TiO_2, (**b**) SnO_2, and (**c**) TiO_2/SnO_2 bilayer ETL structures.

4. Conclusions

This study investigated the properties of different ETLs in PSCs and their impacts on device performances. The TiO_2, SnO_2, and TiO_2/SnO_2 bilayer ETLs were compared by analyzing their surface morphology, current leakage, and carrier transport behavior. The results showed that the TiO_2/SnO_2 bilayer ETL owned the lowest current leakage and the most efficient carrier transport between PVSK and ETL, leading to the higher FF and efficiency of the PSCs.

This study also used PL and TR-PL analyses to investigate the carrier recombination properties of PVSK films grown on different ETLs. The results showed that the TiO_2/SnO_2 bilayer ETL can effectively suppress carrier recombination and improve carrier transport, leading to higher PCE and FF values of PSCs.

In addition, the dark current of the PSCs was analyzed, which showed that the PSCs with the TiO_2/SnO_2 bilayer ETL had the lowest dark current, indicating better charge carrier extraction and lower recombination losses. Overall, the study demonstrated that the use of a TiO_2/SnO_2 bilayer ETL can significantly improve the performance of PSCs by reducing current leakage, improving carrier transport, and suppressing carrier recombination. The conversion efficiency of PSCs can be enhanced from 13.58% (TiO_2 ETL) to 20.49% (bilayer ETL).

Supplementary Materials: The following supporting information can be downloaded at: https://www.mdpi.com/article/10.3390/en17040871/s1, Figure S1: The cross-sectional SEM image of PVSK with bilayer ETL on FTO glass.

Author Contributions: The study was a collaborative effort led by R.-Y.H. and Y.-L.L., who provided valuable insights and guidance throughout the research process. R.-Y.H., W.-J.S. and Y.-H.C. carried out the experiment and worked together to collect and analyze the data. R.-Y.H. and Y.-H.C. made significant contributions to the data analysis and manuscript preparation, drawing on their expertise in the field. Throughout the project, Y.-L.L. provided critical feedback and engaged in constructive discussions, helping to refine the research design and interpret the findings. The study benefited greatly from the contributions of all team members, who worked collaboratively to produce high-quality research output. All authors have read and agreed to the published version of the manuscript.

Funding: We express our sincere gratitude for the financial support provided by the Bureau of Energy, Taiwan, under Contract No. 112-S0102. Additionally, we sincerely acknowledge the invaluable support from the National Science and Technology Council, Taiwan, through Grants MOST 109-2221-E-018-014-MY2, MOST 110-2622-E-018-001, MOST 111-2221-E-018-007, NSTC 112-2515-S-018-003, and NSTC 112-2221-E-018-006-MY2.

Data Availability Statement: Data are contained within the article and Supplementary Materials.

Conflicts of Interest: The authors declare no conflict of interest.

References

1. Guo, Z.; Jena, A.K.; Kim, G.M.; Miyasaka, T. The high open-circuit voltage of perovskite solar cells: A review. *Energy Environ. Sci.* **2022**, *15*, 3171–3222. [CrossRef]
2. Zhang, H.; Ji, X.; Yao, H.; Fan, Q.; Yu, B.; Li, J. Review on efficiency improvement effort of perovskite solar cell. *Sol. Energy* **2022**, *233*, 421–434. [CrossRef]
3. Ma, S.; Yuan, G.; Zhang, Y.; Yang, N.; Li, Y.; Chen, Q. Development of encapsulation strategies towards the commercialization of perovskite solar cells. *Energy Environ. Sci.* **2022**, *15*, 13–55. [CrossRef]
4. Kojima, A.; Teshima, K.; Shirai, Y.; Miyasaka, T. Organometal halide perovskites as visible-light sensitizers for photovoltaic cells. *J. Am. Chem. Soc.* **2009**, *131*, 6050–6051. [CrossRef] [PubMed]
5. Jung, E.H.; Jeon, N.J.; Park, E.Y.; Moon, C.S.; Shin, T.J.; Yang, T.-Y.; Noh, J.H.; Seo, J. Efficient, stable and scalable perovskite solar cells using poly (3-hexylthiophene). *Nature* **2019**, *567*, 511–515. [CrossRef]
6. Jiang, Q.; Zhao, Y.; Zhang, X.; Yang, X.; Chen, Y.; Chu, Z.; Ye, Q.; Li, X.; Yin, Z.; You, J. Surface passivation of perovskite film for efficient solar cells. *Nat. Photonics* **2019**, *13*, 460–466. [CrossRef]
7. Basumatary, P.; Agarwal, P. A short review on progress in perovskite solar cells. *Mater. Res. Bull.* **2022**, *149*, 111700. [CrossRef]
8. Jiang, Q.; Zhang, L.; Wang, H.; Yang, X.; Meng, J.; Liu, H.; Yin, Z.; Wu, J.; Zhang, X.; You, J. Enhanced electron extraction using SnO_2 for high-efficiency planar-structure $HC(NH_2)_2PbI_3$-based perovskite solar cells. *Nat. Energy* **2016**, *2*, 16177. [CrossRef]
9. Li, J.; Wen, F.; Wang, S. Perovskite Tandem Solar Cell Technologies. *Energies* **2023**, *16*, 1586. [CrossRef]
10. Saeed, A.; Salah, M.M.; Zekry, A.; Mousa, M.; Shaker, A.; Abouelatta, M.; Amer, F.Z.; Mubarak, R.I.; Louis, D.S. Investigation of High-Efficiency and Stable Carbon-Perovskite/Silicon and Carbon-Perovskite/CIGS-GeTe Tandem Solar Cells. *Energies* **2023**, *16*, 1676. [CrossRef]
11. Srivishnu, K.S.; Markapudi, P.R.; Sundaram, S.; Giribabu, L. Semitransparent Perovskite Solar Cells for Building Integrated Photovoltaics: Recent Advances. *Energies* **2023**, *16*, 889. [CrossRef]
12. Olzhabay, Y.; Ng, A.; Ukaegbu, I.A. Perovskite PV energy harvesting system for uninterrupted IoT device applications. *Energies* **2021**, *14*, 7946. [CrossRef]
13. Zhang, T.; He, Q.; Yu, J.; Chen, A.; Zhang, Z.; Pan, J. Recent progress in improving strategies of inorganic electron transport layers for perovskite solar cells. *Nano Energy* **2022**, *104*, 107918. [CrossRef]
14. Uddin, A.; Yi, H. Progress and challenges of SnO_2 electron transport layer for perovskite solar cells: A critical review. *Sol. RRL* **2022**, *6*, 2100983. [CrossRef]
15. Huang, S.; Li, P.; Wang, J.; Huang, C.-C.; Xue, Q.; Fu, N. Modification of SnO_2 electron transport Layer: Brilliant strategies to make perovskite solar cells stronger. *Chem. Eng. J.* **2022**, *439*, 135687. [CrossRef]
16. Xiong, L.; Guo, Y.; Wen, J.; Liu, H.; Yang, G.; Qin, P.; Fang, G. Review on the application of SnO_2 in perovskite solar cells. *Adv. Funct. Mater.* **2018**, *28*, 1802757. [CrossRef]
17. Hu, M.; Zhang, L.; She, S.; Wu, J.; Zhou, X.; Li, X.; Wang, D.; Miao, J.; Mi, G.; Chen, H. Electron transporting bilayer of SnO_2 and TiO_2 nanocolloid enables highly efficient planar perovskite solar cells. *Sol. RRL* **2020**, *4*, 1900331. [CrossRef]
18. Sun, X.; Li, L.; Shen, S.; Wang, F. TiO_2/SnO_2 Bilayer Electron Transport Layer for High Efficiency Perovskite Solar Cells. *Nanomaterials* **2023**, *13*, 249. [CrossRef]
19. Li, N.; Yan, J.; Ai, Y.; Jiang, E.; Lin, L.; Shou, C.; Yan, B.; Sheng, J.; Ye, J. A low-temperature TiO_2/SnO_2 electron transport layer for high-performance planar perovskite solar cells. *Sci. China Mater.* **2020**, *63*, 207–215. [CrossRef]
20. Shu, H.; Peng, C.; Chen, Q.; Huang, Z.; Deng, C.; Luo, W.; Li, H.; Zhang, W.; Zhang, W.; Huang, Y. Strategy of Enhancing Built-in Field to Promote the Application of C-TiO_2/SnO_2 Bilayer Electron Transport Layer in High-Efficiency Perovskite Solar Cells (24.3%). *Small* **2022**, *18*, 2204446. [CrossRef] [PubMed]
21. Yu, B.; Yu, H.; Sun, Y.; Zhang, J. Dual-layer synergetic optimization of high-efficiency planar perovskite solar cells using nitrogen-rich nitrogen carbide as an additive. *J. Mater. Chem. A* **2022**, *10*, 21390–21400. [CrossRef]
22. Mali, S.S.; Patil, J.V.; Arandiyan, H.; Hong, C.K. Reduced methylammonium triple-cation $Rb_{0.05}(FAPbI_3)_{0.95}(MAPbBr_3)_{0.05}$ perovskite solar cells based on a TiO_2/SnO_2 bilayer electron transport layer approaching a stabilized 21% efficiency: The role of antisolvents. *J. Mater. Chem. A* **2019**, *7*, 17516–17528. [CrossRef]
23. Liu, Z.; Sun, B.; Liu, X.; Han, J.; Ye, H.; Tu, Y.; Chen, C.; Shi, T.; Tang, Z.; Liao, G. 15% efficient carbon based planar-heterojunction perovskite solar cells using a TiO_2/SnO_2 bilayer as the electron transport layer. *J. Mater. Chem. A* **2018**, *6*, 7409–7419. [CrossRef]
24. Abuhelaiqa, M.; Shibayama, N.; Gao, X.-X.; Kanda, H.; Nazeeruddin, M.K. SnO_2/TiO_2 Electron Transporting Bilayers: A Route to Light Stable Perovskite Solar Cells. *ACS Appl. Energy Mater.* **2021**, *4*, 3424–3430. [CrossRef]
25. Khan, J.I.; Isikgor, F.H.; Ugur, E.; Raja, W.; Harrison, G.T.; Yengel, E.; Anthopoulos, T.D.; De Wolf, S.; Laquai, F. Charge Carrier Recombination at Perovskite/Hole Transport Layer Interfaces Monitored by Time-Resolved Spectroscopy. *ACS Energy Lett.* **2021**, *6*, 4155–4164. [CrossRef]
26. Li, C.; Song, Z.; Zhao, D.; Xiao, C.; Subedi, B.; Shrestha, N.; Junda, M.M.; Wang, C.; Jiang, C.S.; Al-Jassim, M. Reducing saturation-current density to realize high-efficiency low-bandgap mixed tin–lead halide perovskite solar cells. *Adv. Energy Mater.* **2019**, *9*, 1803135. [CrossRef]
27. Guo, X.; Du, J.; Lin, Z.; Su, J.; Feng, L.; Zhang, J.; Hao, Y.; Chang, J. Enhanced efficiency and stability of planar perovskite solar cells using SnO_2: $InCl_3$ electron transport layer through synergetic doping and passivation approaches. *Chem. Eng. J.* **2021**, *407*, 127997. [CrossRef]

28. Zhang, Y.-N.; Li, Q.; Li, B.; Wang, C.-X. Insight into structure defects in high-performance perovskite solar cells. *J. Power Sources* **2023**, *570*, 233011. [CrossRef]
29. Khaleda, M.F.; Vengadaesvaran, B.; Rahim, N. Spectral response and quantum efficiency evaluation of solar cells: A review. In *Energy Materials*; Elsevier: Amsterdam, The Netherlands, 2021; pp. 525–566.